15th Australasian Wind Engineering Society (AWES) Workshop
Sydney, Australia
23-24 February, 2012

Wind loads on solar panels in dual-layer offset-plate arrangements.

R. A. Edgar[1], S. Cochard[2], Z. H. Stachurski[1]

[1]College of Engineering & Computer Science
Australian National University, Canberra 0200, Australia

[2]Faculty of Engineering & IT
The University of Sydney, Sydney 2006, Australia

Abstract

Wind-induced loads on flat plates simulating solar panels of tracking systems are analyzed using computational fluid dynamic methods. Tracking systems typically mount photovoltaic panels in contiguous side-by-side relationship. This paper introduces and evaluates new dual-layer offset-plate arrangements that enable vents between layers and plates to alter pressure balance and off-load fluid forces. It is shown 5×5 and 7×7 dual-layer offset-plate arrays have significantly reduced wind-load compared to contiguous arrangements of equivalent area in the 10–33 m^2 range at the structural extreme (array inclination 15° off vertical) under natural log-profile wind conditions.

Introduction

This study arises from interest to reduce wind-load on solar tracking systems deploying photovoltaic (PV) panels. Tracking panels harvest up to 40% more power-producing light than optimally aligned stationary systems, but the structure of tracking mechanisms must be built to support the worst case conjuncture of panel wind-load and orientation.

Research needs to examine whether panel layouts can be improved to reduce wind loads on tracking mechanisms. Doing so can lift productivity of tracking and power generation based on the ubiquitous PV panel. The present investigation compares and contrasts 35 m/s wind loads on contiguous versus dual-layer offset-plate arrangements of 10–33 m^2 PV surface capacity.

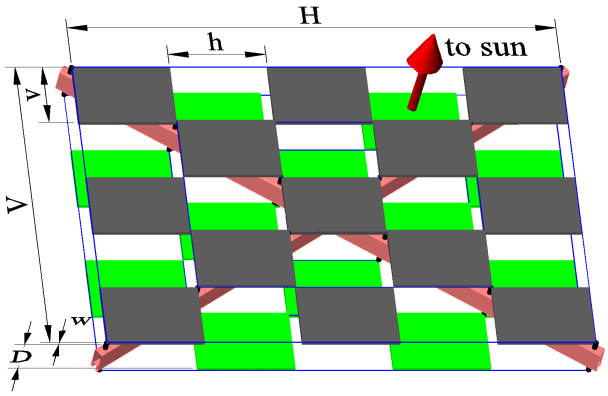

Figure 1: A 5×5 dual-layer offset-plate arrangement.

A dual-layer offset-plate arrangement, of area $H \times V$ and separation D, is shown in Figure 1. Grey upper-layer and green lower-layer plates representing PV panels are shown together with an arrow indicating the sun's direction. Light strikes the $h \times v$ solar panel faces perpendicularly when tracking. Figure 1 shows the offset in plate positions needed between layers to avoid shadow (when tracking), array diagonal cross-members for tracking mechanism attachment and support of through dowels; and a conceptual means of attaching plates to cables strung between dowel ends.

Commercial tracking systems were reviewed for relevant parametric ranges and concluded with the following findings:

- maximum inclination of panel arrays, perpendicular to sun direction, is 15° off vertical;
- dual-axis systems have superior pointing accuracy and range favoured for high efficiency and dual-layer offset-plate arrangements;
- PV surfaces totaling 10–33 m^2 cover most applications; and
- maximum wind speed of specifications is 100 km/h ($\approx$ 35 m/s) with the option of higher wind *survival mode* orientations.

Method

New dual-layer offset-plate arrangements are proposed and compared with industry standard contiguous arrangements using computational fluid dynamic (CFD) methods with Wilcox's k-ω modified Shear-Stress-Transport (SST) model equations (Menter, 1994). The SST model was chosen for best performance versus processor resource requirements. The simulations were carried out using ANSYS CFX-13.

Various array forms, areas ($H \times V$) and layer distances (D) are numerically simulated to compare drag (F_z) and lift (F_y) forces induced by 35 m/s winds.

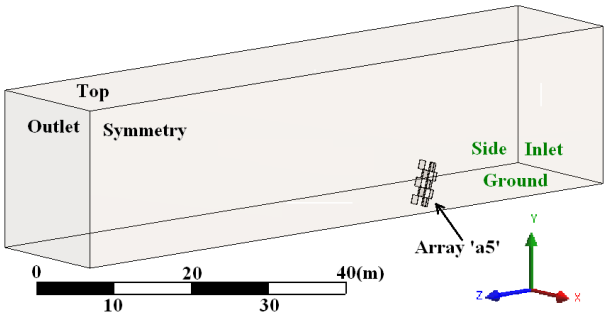

Figure 2: Computational volume with "a5" array form.

Geometry

The analysis domain comprises the symmetric half of a rectangular box with dimensions as follows (see Figure 2):

x-range (crosswind)	6 × [horizontal breadth (H) of enclosed parametric array];
y-range (vertical)	3.5 × [aligned length (V) of enclosed parametric array] + [ground to base-of-array height]; and
z-range (windward)	15 × [aligned length (V) of enclosed parametric array].

Positioned $1/3$ of the way through the domain, via the *inlet* along the z-axis, is one of the following parametrically proportioned array assemblies:

"a1" a 1×1 single flat plate array;
"a5" a 5×5 plate-offset dual-layer array; or
"a7" a 7×7 plate-offset dual-layer array.

The array forms have an azimuth angle (θ) of 180°, i.e. face mean downwind direction, and an elevation angle (ϕ) of 15° off vertical. This is considered the most demanding orientation of arrays for their support system's strength requirements.

The symmetry plane of the computational domain results from it and the array's alignment with the average wind direction, and the isotropic wind stresses of the SST model. Use of symmetry allows half the computational domain to be modeled without information loss, and reduces resource requirements.

From inspection of the dual-layer plate-offset arrangement shown in Figure 1, it can be seen there are:

- an equal number of horizontal and vertical panels, to allow strong inter-layer diagonal cross-members to traverse and support panel arrangements with good load path and minimal shadow on lower-layer (when tracking); and
- an odd number of panels, in order to position a central panel in sunlight above the intersection of supporting cross-members.

The above dot-point features are common to the assessed "a5" and "a7" array forms.

Mesh

The mesh is composed of tetrahedrons, plus wedges in boundary inflation layers. Maximum boundary element face size is 0.8 m on the *ground* and 1.0 m elsewhere. Proximity to *array* sizing is enacted and reduces element side length by an order of magnitude close to *array* edges. A minimum of fifteen inflation layers of expansion ratio 1.1 are present on the *array* and *ground* boundaries. The first inflation layer thickness on the *array* and *ground* are below the y+ = 300 height and are 3mm and 1mm respectively, see Figure 3. The low profiles of inflation layer wedges results in elements of very high skewness but these are accepted because of their reasonably good alignment with flow directions and the needed performance of wall functions between viscous and turbulent wall-boundary sub-layers (ANSYS, 2010, pp.144-145).

Figure 3 shows mesh detail on the lower part of the *symmetry* plane and 33 m^2 "a1" form's side.

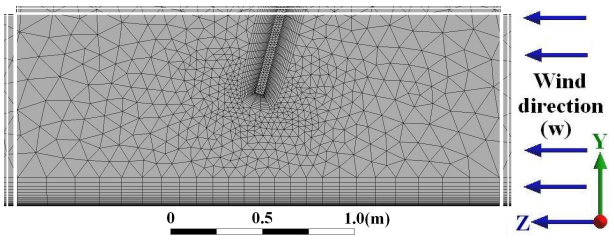

Figure 3: Mesh inflation layers of *ground* and *array* 'walls'.

Mesh statistics of the computational domains of the *large* arrays (i.e. those of $\approx 33\,m^2$ PV capacity frontal area) are shown in Table 1.

As a check of adequate mesh scale refinement, the initial boundary layer heights, their expansion rate, and boundary-element maximum side-lengths are halved in the computational domains of the five "a1" array form sizes examined, and the CFD reported forces found to differ by less than 1% from those of the standard mesh analyses.

Array	"a1": 1×1	"a5": 5×5	"a7": 7×7
Nodes	749,177	3,864,642	4,206,473
Elements	2,867,366	2,328,422	2,500,523

Table 1: Mesh statistics of computational volumes

Boundary conditions

The computational domain has six outside boundaries. The *top* and *side* of the computational domain are "openings" with zero entrainment average relative pressure and turbulence gradient. Mirror symmetry is imposed on the *symmetry* plane of the computational domain. The *ground* "wall" roughness (y_0) is 0.11 m, and the *outlet* has zero average static pressure. The *Array* surface boundaries are smooth walls and all plates modeled are 46 mm wide.

The *input* mean wind velocity ($\overline{w}_\infty$) is given by Equation 2 described below. Velocity Equation 1 exhibits standard atmospheric boundary layer variation with height (y) and ground roughness (y_0) (Stull, 1999, p.382). Velocity Equation 2 is derived from Equation 1 by setting the friction velocity (u_*) to obtain the undisturbed flow velocity $\overline{w}_\infty = 35\,$m/s at a level 5 m above ground. This latter Equation 2 mean wind velocity function for $\overline{w}_\infty$ is subsequently referred to as the '35 m/s' profile or condition.

$$\overline{w}_\infty = \frac{u_*}{\mathrm{K}} \ln \frac{y+y_0}{y_0}; \qquad \text{where } \frac{u_*}{\mathrm{K}} = \frac{\text{(Friction velocity)}}{\text{(von Kármán const.)}} \quad (1)$$

and

$$\overline{w}_\infty = 9.12\,[\mathrm{m/s}] \ln \frac{y+y_0}{y_0}; \qquad \text{for } \overline{w}_\infty|_{y=5\mathrm{m}} = 35\,\mathrm{m/s}. \quad (2)$$

While the scope of the parameter space to be investigated for solar tracking might include any:

- number of layers;
- shape, size and arrangement of plates in non-occluding layers;
- layer envelopes; and
- array positions including orientations;

only dual-layer arrangements of square plates in worst load orientation for retention by tracking support systems are reported.

The worst case scenario, for maximum wind force on arrays, is considered to be when plates are struck from behind by '35 m/s' winds while closest to perpendicular, which from review of commercial tracking systems is 15° off vertical. Rear entrant winds are considered more structurally significant than frontal winds for design because of the high lift forces the former generate on arrays, and in particular the impact of this on the stability of tracking support systems.

Convergence conditions

Plates at high angles to even modest winds initiate flow separation along their edges and have highly turbulent wakes. Although the mean velocity and plate forces of such wakes are low, their transient nature adds to momentum residuals of steady-state analyses. None-the-less, momentum convergence to 10^{-5} rms was generally achieved and to $< 10^{-4}$ rms otherwise. For the latter convergence range, their drag and lift forces were inspected to verify transient oscillations were of negligible amplitude (i.e $<1\%$) and drift (i.e. $<1\%$ over 25 psuedo timesteps).

Results

Preliminary

Associated with the atmospheric Boundary Layer (BL), a question arises as to whether air channeled down or wedged between the array and ground, of the "a1" form in particular, might impose inequitable secondary effects and compromise results of direct comparisons between forms. A CFD atmospheric BL survey of the *large* "a1" form at various ground to base-of-array heights (y_1) was undertaken to resolve this question and inform the eventual choice of $y_1 = 0.6\,\text{m}$ for subsequent comparative analyses.

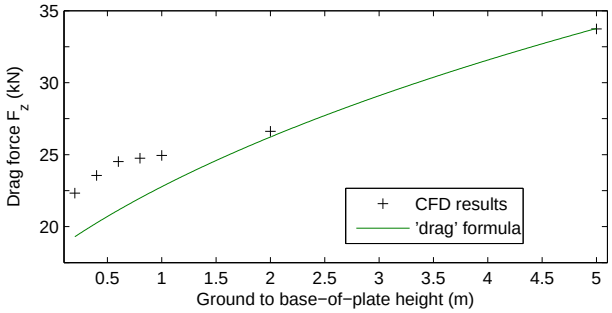

Figure 4: Ground effect on 33 m^2 "a1" form with '35 m/s' wind.

Figure 4 shows "a1" BL survey results for $0.2\,\text{m} < y_1 < 5\,\text{m}$ and a line given by the Equation 4 drag formula described below. Equation 4 correlates well with CFD results for $y_1 > 2\,\text{m}$, but doesn't take into account ground effects and is $\approx 25\%$ below CFD results for $y_1 < 0.6\,\text{m}$.

Drag formula Equation 4 is derived from the basic fluid force Equation 3:

$$F = \frac{1}{2} C \rho A \overline{w}^2 \tag{3}$$

where F = body force; A = body frontal area; ρ = fluid density; $\overline{w}$ = mean velocity; C = dimensionless coefficient;

by taking into account,

- the $\overline{w}_\infty$ vertical wind profile of Equation 2;
- the body frontal area of plate ($A = HV\cos\phi$);
- drag force component ($F_z = F\cos\phi$);

and integrating infinitesimal vertical elements, i.e.

$$\begin{aligned} F_z &= \frac{1}{2}\rho H C_D \cos^2(\phi) \int_{y_1}^{y_2} \left(9.12\,[\text{m}\cdot\text{s}^{-1}] \ln\frac{y+y_0}{y_0}\right)^2 dy \\ &= 36.9\,[\text{N}\cdot\text{m}^{-1}] \left[\frac{y_2+y_0}{y_0}\left(\left\{\ln\frac{y_2+y_0}{y_0} - 1\right\}^2 + 1\right) \right. \\ &\qquad \left. - \frac{y_1+y_0}{y_0}\left(\left\{\ln\frac{y_1+y_0}{y_0} - 1\right\}^2 + 1\right) \right] \end{aligned} \tag{4}$$

where $C_D = 1.27$; $\rho = 1.185\,\text{kg}\cdot\text{m}^{-1}$; $H = V = 5.75\,\text{m}$; $y_0 = 0.11\,\text{m}$; y_1 = "a1" ground to base-of-array height; $y_2 = y_1 + V\cos\phi = y_1 + 5.55\,\text{m}$.

The Equation 4 drag coefficient $C_D = 1.27$ is consistent with the 10% turbulence conditions of the BL survey given that:

- the drag coefficient (C_D) for square plates is $\approx$1.17 for low turbulence subsonic flows with Reynolds numbers $> 10^4$ (Smith and Whipple, 1934, p.27);
- the Equation 3 provides reasonable results for vector force components when plate angles are in the range 0°–45° off vertical (Hoerner, 1951, 2nd Ed. 1965, p.3-16); and
- the drag coefficient of plates increases by up to 7% with lesser turbulence (Schubauer and Dryden, 1935).

Note drag formulas 3 and 4 don't account for atmospheric BL effects while CFD results do. Figure 4 thus displays BL and wedge effects in the observed difference between formula and CFD results. That difference is positive but appears too minor and consistent for $y_1 < 0.6\,\text{m}$ to suggest wedge effects are particularly unique or severe on the "a1" form. As a check, wind from the opposite direction ($\theta = 0°$) was examined; the flow is then directed upwards and away from the ground without wedging effects. The "a1" form with $\theta = 0°$ and $y_1 = 0.6\,\text{m}$ has 5.5% higher CFD drag than found with $\theta = 180°$. Rather than revealing extreme secondary effects of flow beneath the "a1" form then, this result shows that flow paths directed down into low velocity ground layers are easier on arrays than flows directed up into high velocity upper layers, and special care to manage exceptional condtions when making comparisons is not required.

Comparative

Four "a5" and "a7" layer distances (D) = [300, 450, 600, 750] were investigated for '35 m/s' wind conditions with 10% turbulence. Five CFD analyses were run for each layer distance to cover the 10–33 m^2 range, i.e. forty CFD analyses for these two forms in all. CFD results showed near linear growth of drag and lift forces with plate area as shown in Figures 5 and 6, however a 1%–2% dip in force appears in area midranges. When fitting results a quadratic formula was used to conserve that feature.

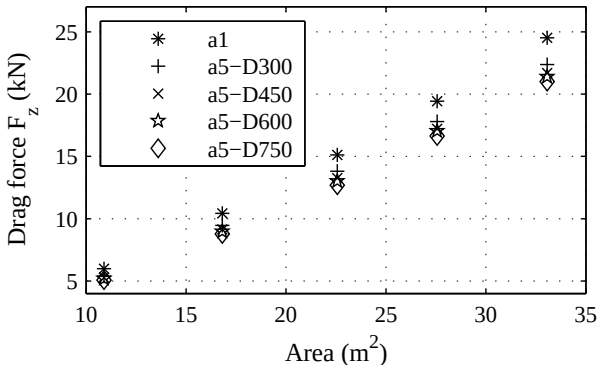

Figure 5: Drag on "a1" and "a5" forms by '35 m/s' winds.

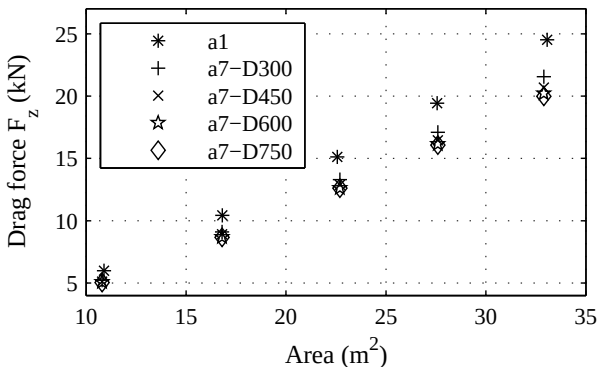

Figure 6: Drag on "a1" and "a7" forms by '35 m/s' wind.

CFD resultant drag forces are shown together with "a1", for "a5" and "a7" forms in Figures 5 and 6 respectively. Relevant layer distance (D) of results figure in legend suffixes. Drag

forces fall as layer distance is increased to 750 mm. Being considered impractical for solar applications the layer distance of minimum drag (beyond 750mm) was not covered.

Figure 7 shows CFD drag results for "a1", and for "a5" and "a7" with D=750 mm. A quadratic curve has been fitted to the "a7" drag results, and a dashed curve 21% higher. The dashed curve can be seen to fall close to the results for "a1". This suggest a given tracking mechanism may carry 21% more PV area by adopting an "a7" rather than "a1" contiguous plate form.

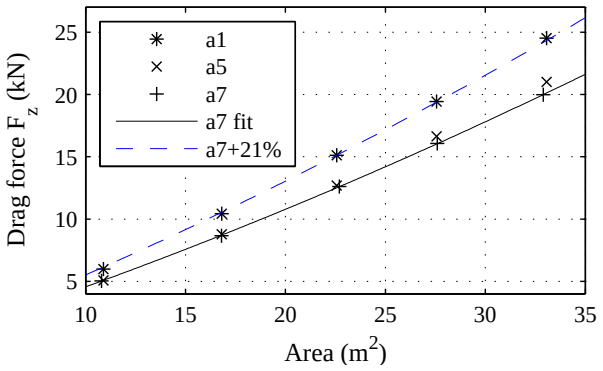

Figure 7: Drag on arrays with $D = 750$ mm in '35 m/s' wind.

Figure 8 shows lift results for "a1", and for "a5" and "a7" with D=750 mm. A quadratic curve has been fitted to "a7" lift results, and a dashed curve 31% higher. The dashed curve can be seen to fall close to the results of "a1". This suggests tracking mechanisms may experience 31% less lift by adopting an "a7" arrangement rather than contiguous "a1" form.

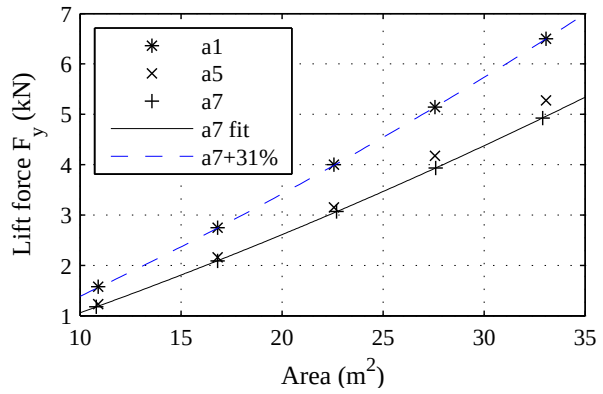

Figure 8: Lift on arrays with $D = 750$ mm in '35 m/s' wind

Total pressure on the symmetry plane of the *large* "a7" and "a1" forms are shown in Figures 9 (A) and 9 (B) respectively.

Pressure collapses behind perpendicularly held plates in flows having Reynolds numbers $\gtrapprox 10^4$ resulting in high form drag. This collapse is clearly evident in the pressure differential across plates of Figure 9. With '35 m/s' winds, viscous (or tangential) forces on surfaces are many orders of magnitude less than pressure contributions to force. Viscous and pressure force terms of analyses are reported in CFX output and results confirm viscous contributions are 3–4 orders of magnitude less than pressure contributions for all array forms in the parametric ranges investigated.

The resultant force on plates can then be approximated by the unbalanced normal forces (or pressure integral) across plates. Figure 9 B shows the *large* "a1" single plate has $\approx$ 600Pa pressure over its upwind face and $\approx$-150 Pa pressure over its downwind side. This net 750 Pa pressure over 33 m^2 would produce a force of 24.8kN, with drag and lift components of 24.0kN and 6.5kN respectively, and is similar to the *large* "a1" results indicated in Figures 5 to 8.

The Figure 9 A shows an intermediate pressure balance is established between front and rear layers of "a7". This intermediary pressure within a dual-layer offset-plate arrangement reduces net forces relative to those of the contiguous "a1" plate form.

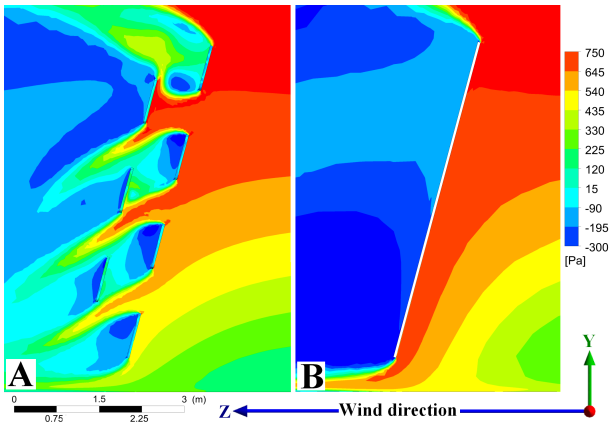

Figure 9: Total pressure on the symmetry plane of *large* (A) "a7" and (B) "a1" forms.

Conclusions

In the case of dual-layer offset-plate arrangements:

- negative pressure on trailing face of upwind layer is mitigated by positive pressure on leading face of downwind layer. This reduces pressure differential across upwind layer plates and therefore their contribution to net force; and similarly
- positive pressure on leading faces of downwind layer is reduced by shielding effect of upwind layer. This reduces pressure differential across downwind plates and therefore their contribution to net force.

As a result of favourable pressure redistributions by dual-layer offset-plate arrangements, the efficiency of solar tracking systems using the ubiquitous PV panel may be significantly improved. In the parametric range of interest to solar tracking, CFD results show wind induced drag and lift (affecting required tracking system strength, anchorage and weight) can be reduced by as much as 21% and 31% respectively by separating PV panels on and in layers. *

References

ANSYS (2010) ANSYS CFX-solver modeling guide - release 13.0. ANSYS Inc.

Hoerner SF (1951, 2nd Ed. 1965) Fluid-dynamic drag. S.F.Hoerner

Menter FR (1994) Two-equation eddy-viscosity turbulence models for engineering applications. American Institute of Aeronautics and Astronautics Inc 32(8):1598–1605

Schubauer GB, Dryden HL (1935) The effect of turbulence on the drag of flat plates. NACA Technical Report (546):129–133

Smith RH, Whipple JVH (1934) Air force measurements on bodies moving through still air. The Journal of Aeronautical Sciences 1:21–27

Stull R (1999) An introduction to boundary layer meteorology. Kluwer Academic Pulblishers